6th World Congresses of Structural and Multidisciplinary Optimization
Rio de Janeiro, 30 May - 03 June 2005, Brazil

Design Optimization of a Submerged Entry Nozzle for Minimum Meniscus Turbulent Kinetic Energy

K.J. Craig, L.J. Haarhoff, C.A. Pretorius, G.J. de Wet

Multidisciplinary Design Optimization Group (MDOG), Department of Mechanical and Aeronautical Engineering,
University of Pretoria, Pretoria 0002, South Africa. ken@up.ac.za

1. Abstract
The paper describes the process to determine the optimum parameters of a Submerged Entry Nozzle (SEN) for minimum meniscus turbulent kinetic energy (i.e., stable meniscus) during the continuous casting of stainless steel slabs. Design variables include the port angle, port height and well depth of the SEN, while the effect of submergence depth is investigated. The SEN is designed for a width range of 1000 mm to 1300 mm, and a casting speed of 1.3 m/min.
The Computational Fluid Dynamics (CFD) analysis of the mold and SEN for two slab widths is performed using the k-ω turbulence model and dynamic adaption of the mesh as in Fluent. The grid generation process is fully parameterized for twelve possible design variables and completely automated. The optimization is performed using LS-OPT's Central Composite experimental design with 17 design points for the 3 design variables. Different objective functions are considered because of the transient nature of the mold and SEN flow field. Due to the high cost of the function evaluations, only one design iteration is performed.
The CFD model is validated using water model results obtained with the University of Pretoria's 40% mold water model. The validation results show very good agreement of both the base and improved design between the CFD and water model. Fluent is used as the CFD solver.
A limited investigation is performed of the robustness of the improved design. The results show that the standard deviation of the responses is about 10% for all the responses when specifying the tolerances on the design variables expected during the manufacture of the SEN.
2. Keywords: Continuous caster submerged entry nozzle, optimization

3. Introduction
Computational modeling of continuous caster components [1-7] has been used for the last decade to supplement traditional experimental methods such as water modeling and plant trials [8-12]. As computational models have matured in both validity and their ability to model more complex features, they have presented the opportunity to enhance the traditional trial-and-error analyses by using more systematic approaches such as design optimization.
The tundish was chosen as the first candidate for design optimization as it is easier to model [13, 14], both from a water modeling and a computational perspective. In addition, the role of the tundish in the continuous casting process has evolved from that of a reservoir to being a grade separator and an inclusion removal device. For both grade separation and inclusion removal, the flow patterns inside the tundish play an important role. For the former, the flow patterns determine the amount of mixing that occurs, while for the latter, the paths of inclusion particles are influenced by the flow field. Several tundish designs and tundish devices or furniture exist that have as their aim the modification of tundish flow patterns, to either minimize mixed-grade length during transition, and/or to increase inclusion particle removal by the slag layer. Because of the often conflicting objectives and freedom in the selection of design variables, design optimization of the tundish furniture is indicated. An impact pad will be used as a representative refractory component in this study.
The continuous caster process that follows the tundish is the mold. Liquid steel enters the mold through a Submerged Entry Nozzle (SEN), the design of which has a primary influence on the flow pattern in the mold and the resultant steel quality. The liquid steel then solidifies through mold and spray cooling. The SEN controls the speed, shape and direction of the jet. Its performance is usually analyzed by considering liquid flow only, especially as buoyancy effects due to superheat is negligible [4]. The other reason why SEN design is an attractive topic is the fact that it is a relatively inexpensive part in the continuous caster machinery that can easily be changed. A SEN design that ensures a quiet meniscus is desirable as slag powder entrainment by the SEN jet is limited.
The next section will describe the Computational Fluid Dynamics (CFD) modeling that was performed for the two components, as well as validation of the SEN analysis. This will be followed by a description of the optimization method used. The results of the optimization are presented next with discussion. Conclusions drawn from the results conclude the paper.

4. CFD Modeling
The CFD modeling process involves parameterization of a geometry, mesh generation and solution of the fluid flow and heat transfer equations. The commercial CFD code, FLUENT [15] with its pre-processor GAMBIT [16] is used in this study. The scripting capability of both codes is used to automate the design optimization process in the form of journal files.
As an example of the capabilities of the parameterization, consider the different SEN geometries in Figure 1.

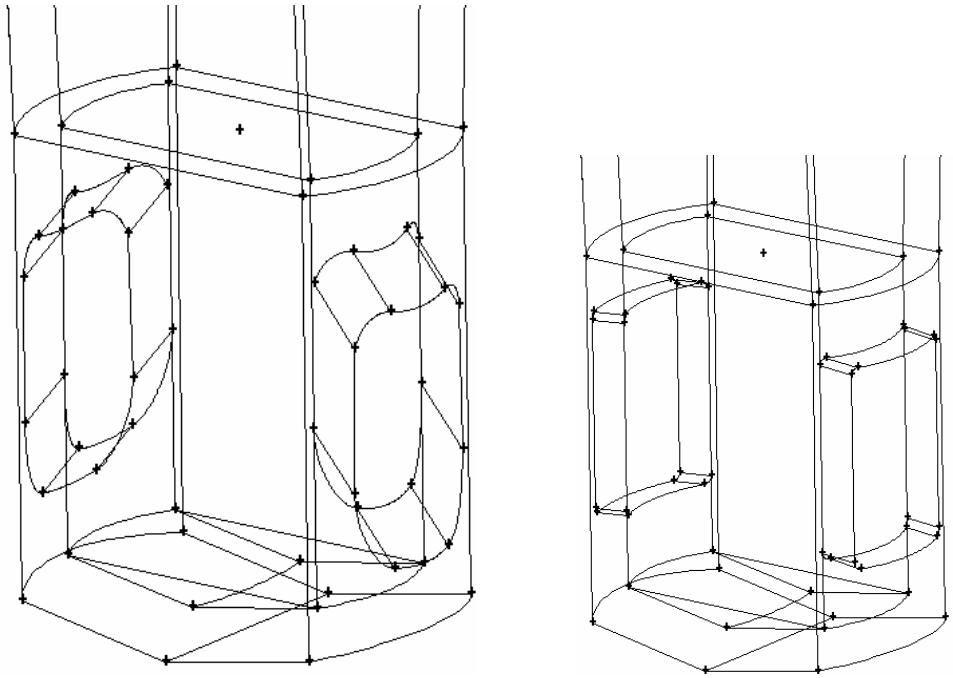

Figure 1. Different SEN geometries illustrating parameterization

The grid generation and CFD solution process is driven using the design optimization software LS-OPT [17]. For the simulations presented in this paper, the Reynolds Averaged Navier-Stokes equations are solved with the k-ε (tundish) and k-ω (SEN) turbulence model providing the turbulent closure. In the SEN model, dynamic grid adaption based on velocity gradients is used to limit the mesh size while still capturing the SEN jet shear layer.

The SEN geometry, mesh and design variables are shown in Figure 2. A symmetric quarter model is used, with hexahedral cells throughout. Although only three design variables as well as the submergence depth of the nozzle are varied in this paper, 12 SEN parameters are included in the parameterization. The boundary conditions used are given in Figure 3. Note that heat transfer is included in the simulation to allow for future constraints involving temperature. The values of maximum velocity magnitude and maximum turbulent kinetic energy on the meniscus are written to file for post-processing.

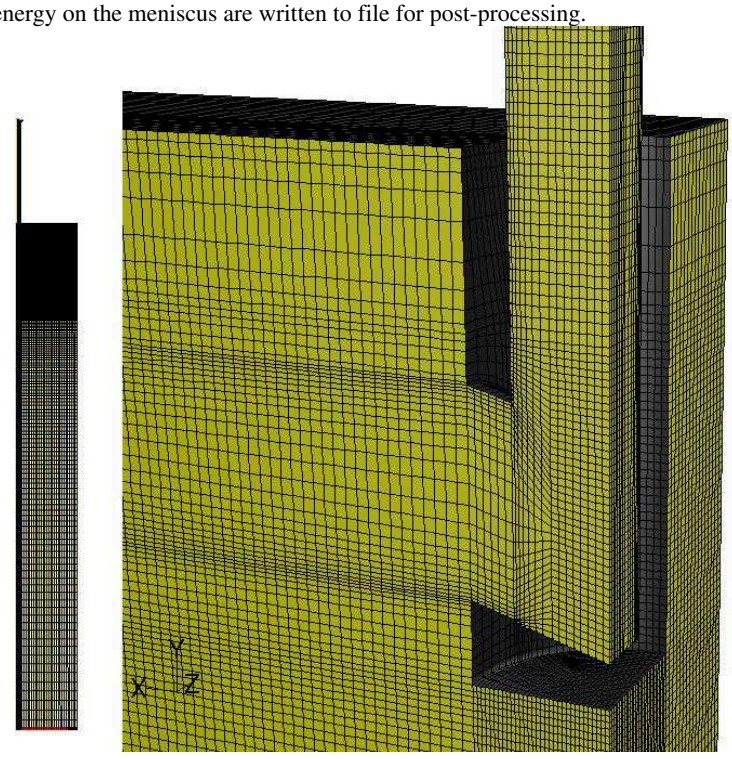

a) b)

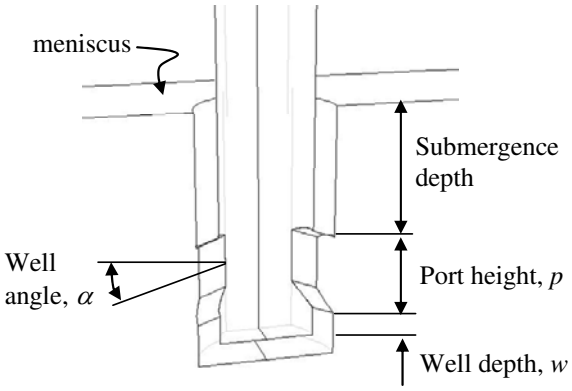

c)

Figure 2. Typical geometry and mesh used for SEN/mold model – a) whole model; b) close-up of SEN c) SEN geometry and design variables

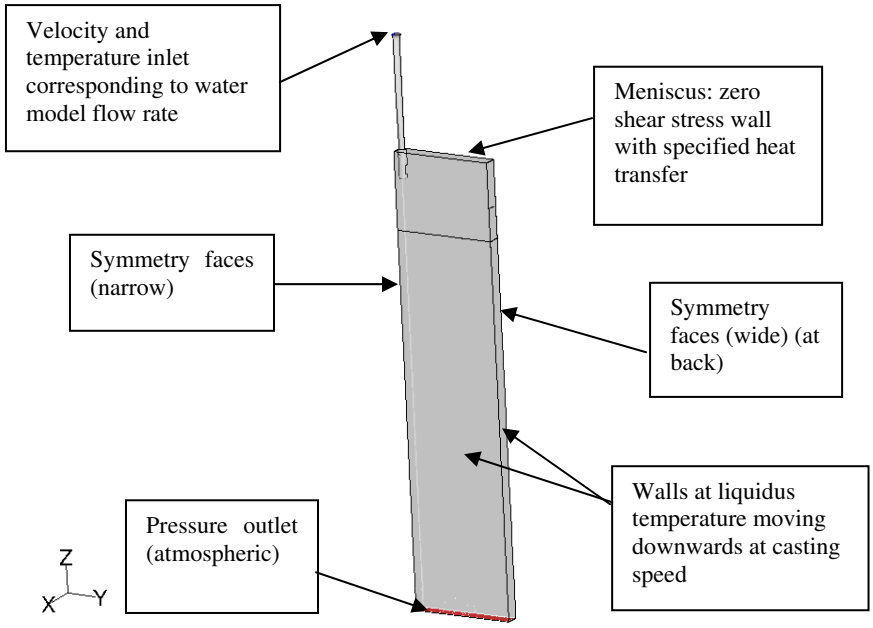

Figure 3. Boundary conditions used for SEN/mold

When separating the SEN from the mold (as some authors do), solutions seem to be more stable and converge quickly to predetermined criteria. However, when evaluating only the SEN, a pressure outlet boundary condition is applied to the SEN where it exits into the mold cavity. The pressure will be assumed to be the ferrostatic pressure due to the submergence depth of the SEN below the meniscus. The flow is then solved and the velocity profile of the SEN exit nozzle is applied as a velocity inlet boundary for the mold in a separate simulation. However, when measuring (in a SEN and mold combined CFD model after convergence) the pressure distribution on the SEN port face, a non-constant pressure distribution is observed. The static and dynamic pressure distributions are illustrated in Figure 4 to show the importance of evaluating the SEN and mold together in one CFD model.

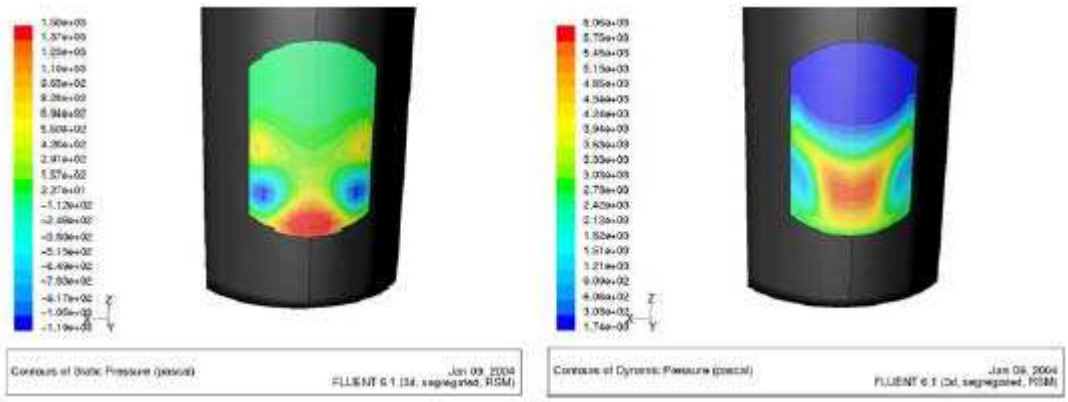

Figure 4. Static and dynamic pressure distribution in 3D SEN port face (quarter model)

The material properties used are listed in Table 1.

Table 1. Table of material properties

Thermal expansion coefficient	0.1107×10^{-3}
Reference density	6975 $kg.m^{-3}$
Reference temperature	1500 °C
Specific heat of liquid steel	817.3 $J.kg^{-1}.K^{-1}$
Conductivity of liquid steel	31.0 $W.m^{-1}.K^{-1}$
Dynamic viscosity of liquid steel	0.0064 Pa.s

4. Experimental Validation of SEN CFD Modeling

The experimental validation of the SEN CFD model was performed using an in-house 40% scale water model. Because of the scale of the model, both Reynolds and Froude similarity cannot be satisfied. As the SEN jet was determined to be fully turbulent at the Froude similarity flow rate, this flow rate was used. A sample validation is shown in Figure 5 in the form of water model dye visualization and path lines obtained from the CFD model. Note how the jet centerlines coincide exactly.

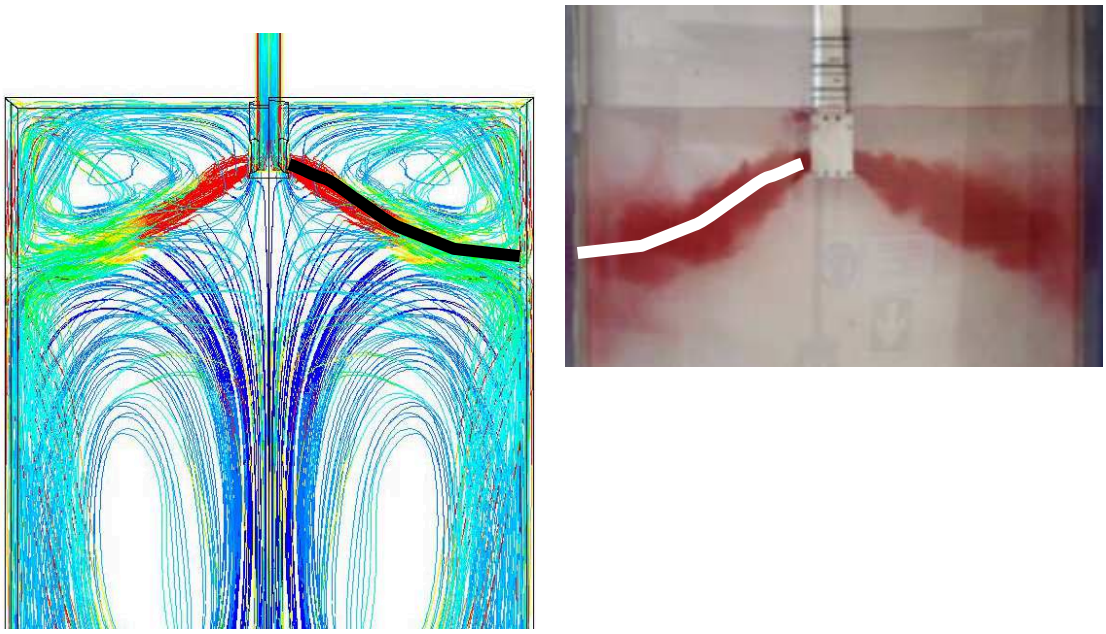

Figure 5. Validation of CFD model using 40% scale water model (Pathlines coloured by vorticity magnitude (Width 1250mm, 2.3m^3/h flow rate, SEN submergence 80mm)) – Improved design

5. Description of Optimization Process

A Central Composite experimental design, as implemented in LS-OPT[17], is used to ensure sampling of 'corners' of the design space. Global response surfaces are constructed due to the high cost of obtaining function values.

The optimization formulation is described as:

$$\begin{gathered} \textit{Variables } \boldsymbol{x} = [x_1, x_2, x_3]^T \\ x_1 = \alpha = \text{SEN port angle} \\ x_2 = p = \text{SEN port height} \\ x_3 = w = \text{SEN well depth} \end{gathered} \tag{1}$$

$$\begin{gathered} \textit{Objective:} \\ \min\ [f(x) = (\text{Max\_TKE\_1060\_80} + \text{Max\_TKE\_1250\_80})*1000 + \\ (\text{Max\_VelMax\_1060\_80} + \text{Max\_VelMax\_1060\_80})*10] \end{gathered}$$

$$\begin{gathered} \textit{Bounds:} \\ x_1 \in (-20;15)^\circ \\ x_2 \in (30;80)\text{mm} \\ x_3 \in (1;40)\text{mm} \end{gathered}$$

The objective is a weighted multi-objective, weighing the maximum velocity and turbulent kinetic energy on the meniscus surface of a narrow mold (1060mm) and that of a medium width mold (1250mm). The shallowest submergence (80mm) is used as a worst-case scenario as far as the jet disturbing the free surface (meniscus) is concerned. Scaling is applied to ensure that the velocity is of the same order as the turbulent kinetic energy (TKE).

6. Optimization Results

6.1 Objective function data

Due to the inherently unsteady nature of a nozzle jet emanating into a cavity, it was problematic to obtain steady-state converged results for all SEN designs. An example of a 'bad' design and a 'good' design is shown in Figure 6, with the stochastic behavior of a 'bad' design (Figure 6a) in the responses with solution iteration indicating the tendency of the jet to be transient, thereby leading to high turbulence and meniscus surface velocities. A 'good' design on the other hand (Figure 6b), exhibits little variation, land in general a lower mean value. Both these plots show the TKE iteration history of 'probe' points on the meniscus surface.

6.2. Design space exploration

Both linear and quadratic polynomial approximations were fitted to 16 experiments as well as the base design for the 3 design variables. The predicted results were simulated and are denoted as 2.1_linear and 2.1_quadratic in Figure 7, where the multi-objective (2) is plotted for all the sampled experiments. Note that the base design has a low multi-objective value, but that the linear approximation improved on this weighted performance. Only one design iteration was performed for this case due to the high cost of the function evaluations (1 week each on a 3GHz linux workstation).

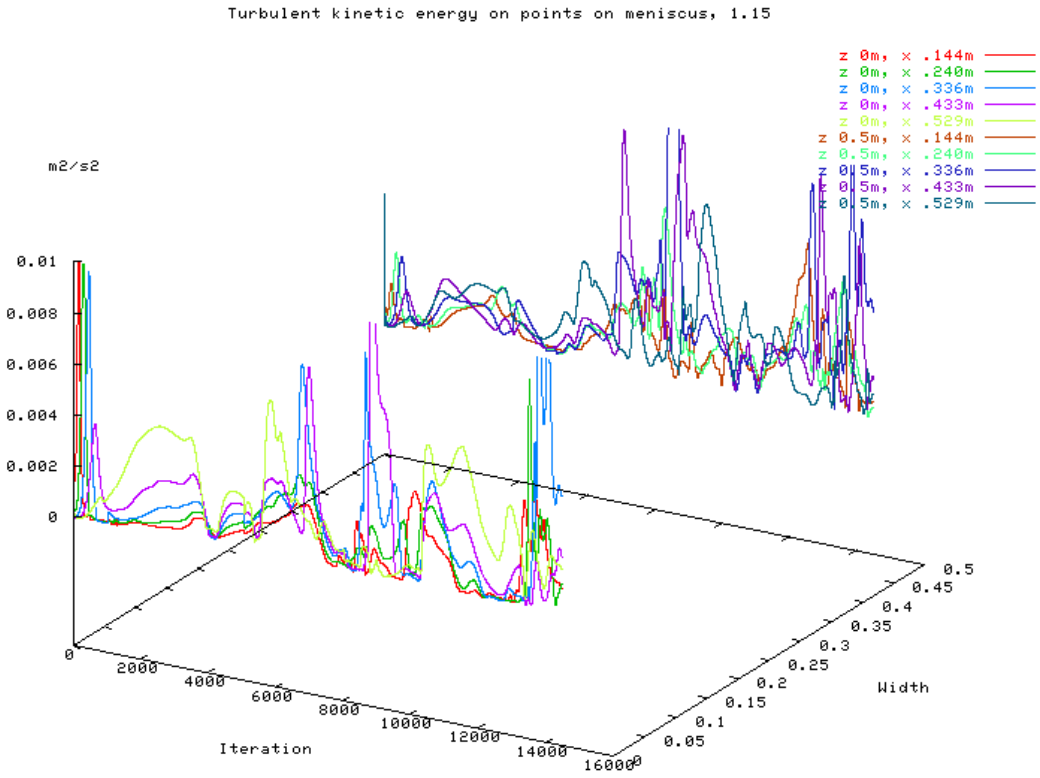

(a)

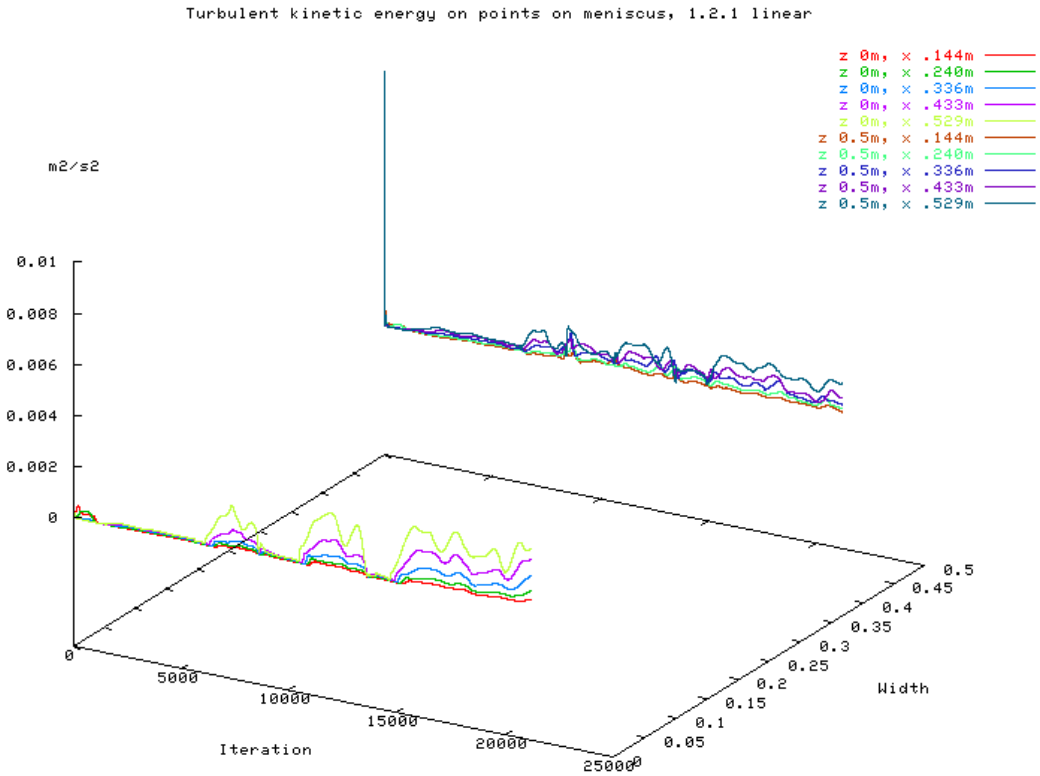

(b)

Figure 6. a) 'Bad' SEN design b) 'Good' SEN design

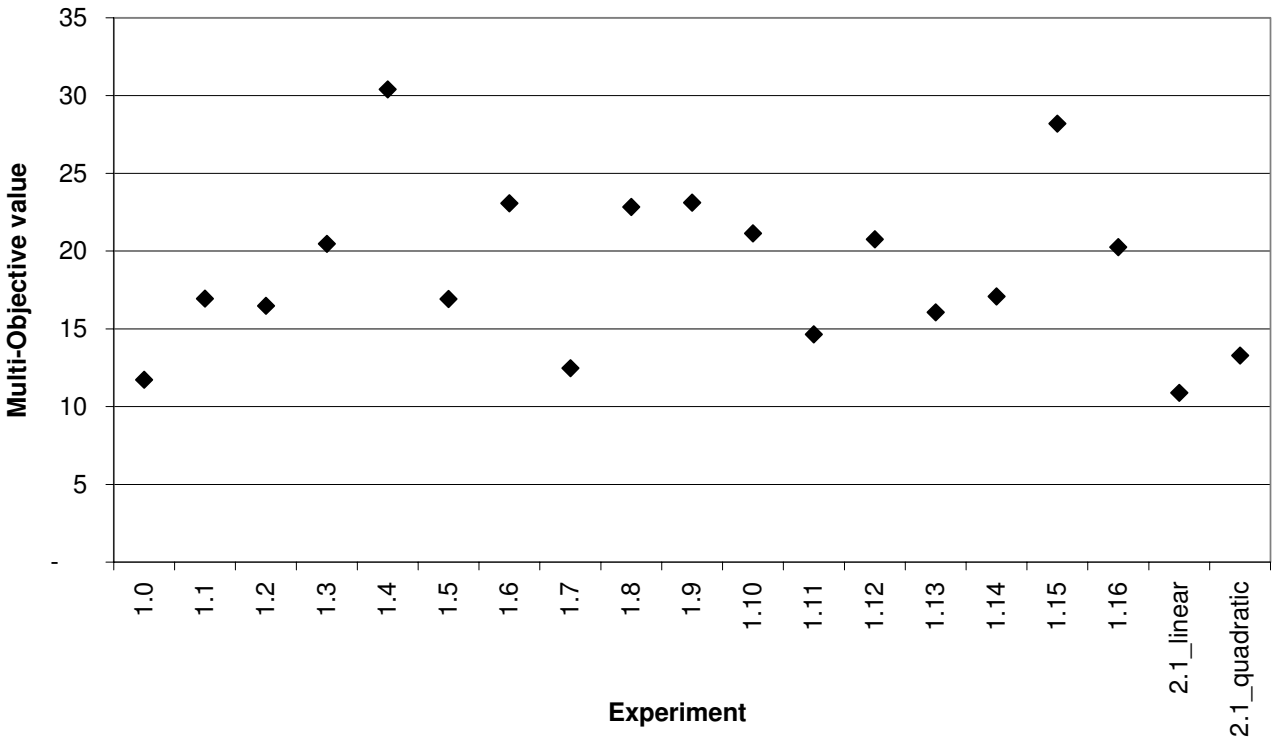

Figure 7. Multi-objective values for experimental design evaluated

6.3. Reliability of base and improved design

To at least provide an indication of the performance of the 2.1_linear improved design relative to the base design, the designs were perturbed using a local space-filling [17] experimental design of 5 experiments (range 4mm and 4°, standard deviation 1mm and 1° for the height and angle, respectively) in two of the design variables (the third (well depth) had reached one of the specified bounds). The location of the design points around the improved design are shown in Figure 8.

Neural network metamodels [17] were fitted through the 2.1_linear and 5 surrounding points and sampled using 1 million Monte Carlo evaluations on a 3 sigma range. The standard deviation of the responses (maximum turbulent kinetic energy on meniscus and maximum velocity magnitude on meniscus for 1250mm and 1060mm widths) were less than 10% of the mean for all responses for the 2.1_linear design (See Figure 9 for TKE frequency distribution at 1250 width as example). The multi-objective components of these perturbed designs are shown in Figure 10, together with the design exploration results, illustrating how the improved design is superior in terms of its robustness (lower values of the multi-objective components for all the perturbations as opposed to the base design 1.0) (where local perturbations, i.e., in one variable at a time, as well as 5 space-filling points around the base design, were evaluated).

6.4. Influence of submergence depth

The submergence depth of the SEN was taken as 80mm in all the results presented so far. This is the shallowest position of the nozzle during casting, and because of the proximity to the meniscus free surface, this had presented a worst-case value for this parameter. To assess the off-design performance of the improved SEN, the submergence depth was varied from the design value of 80mm, to 150mm and 200mm for the improved case. This variation did not adversely affect the design performance (rightmost values in Figure 10). The geometry of the improved design is depicted in Figure 11. A 40% scale model of the improved design was manufactured and tested in the University of Pretoria mold water model. The agreement between the CFD and water model dye visualization of this improved design was shown in Figure 5.

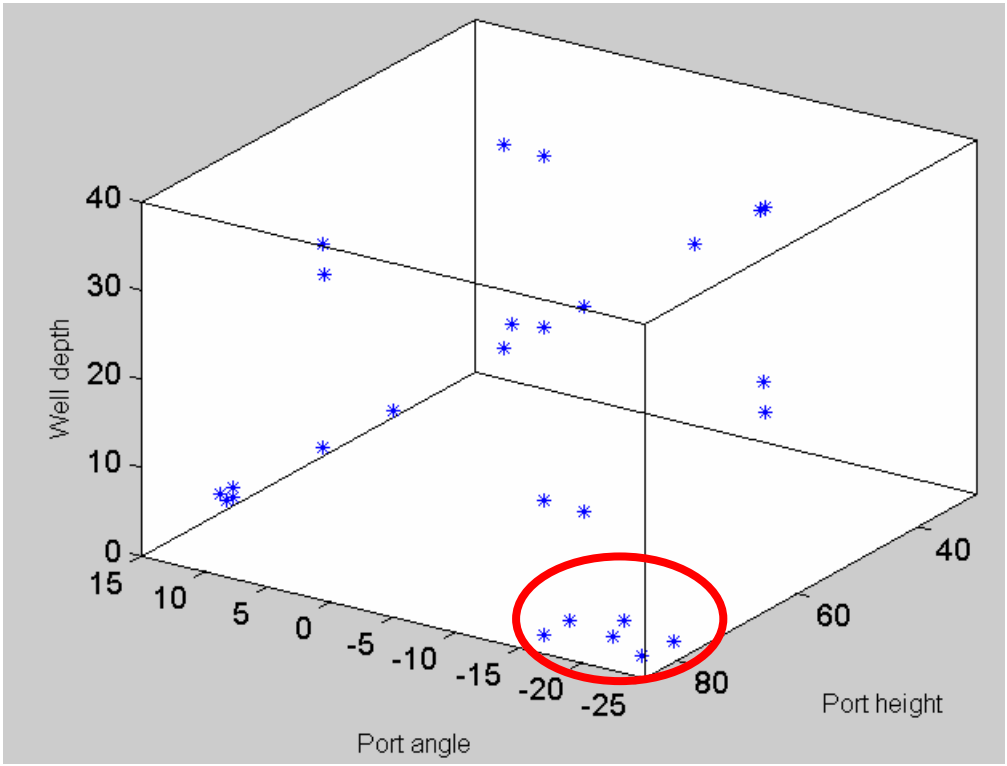

Figure 8. Location of reliability points for base and 2.1_linear designs

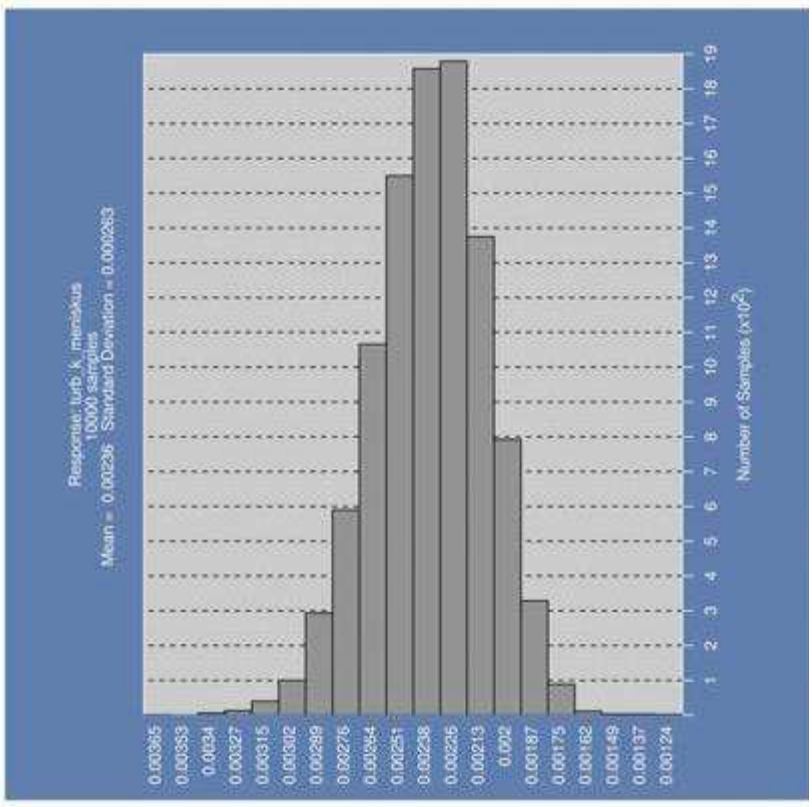

Figure 9. Frequency distribution of maximum turbulent kinetic energy on meniscus [m/s^2] – 1250mm width: Neural Network fit[17]

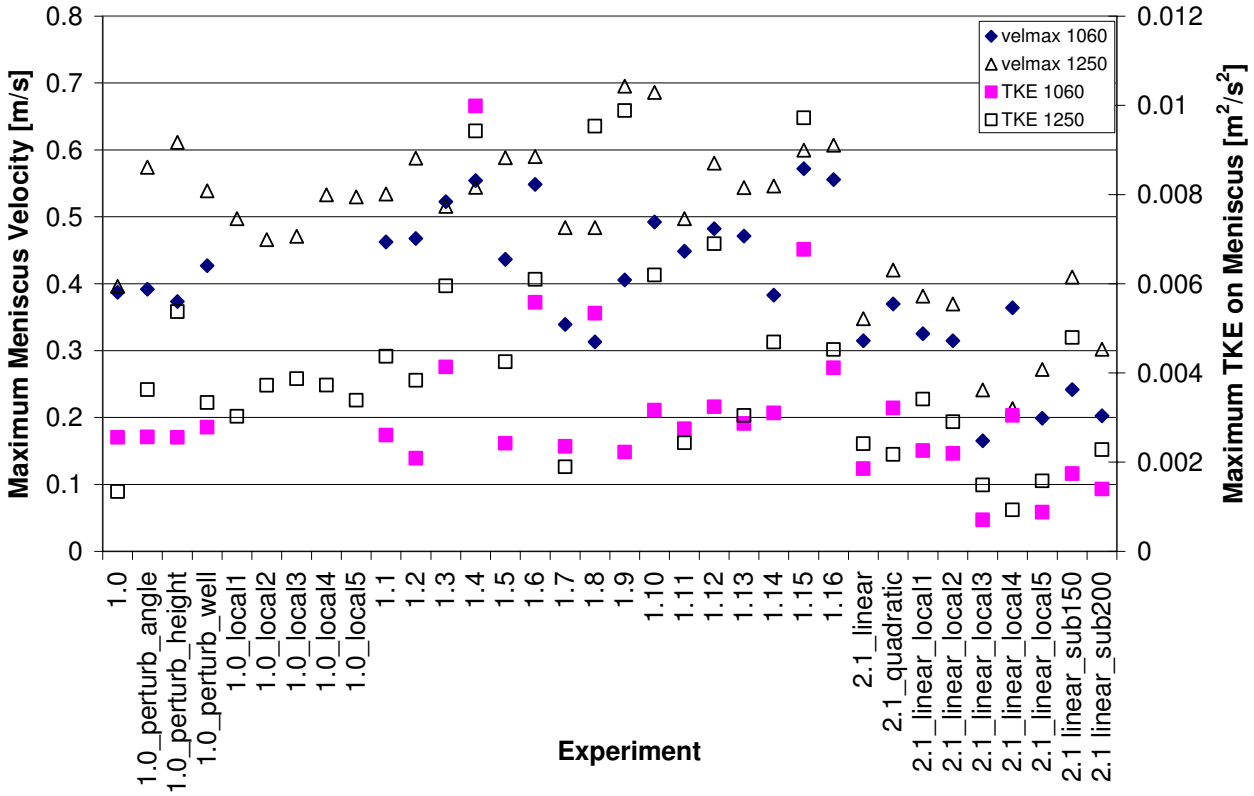

Figure 10. Multi-objective components (maximum velocity and turbulent kinetic energy on meniscus) values for experimental designs and perturbation of base (1.0) and improved (2.1_linear) designs

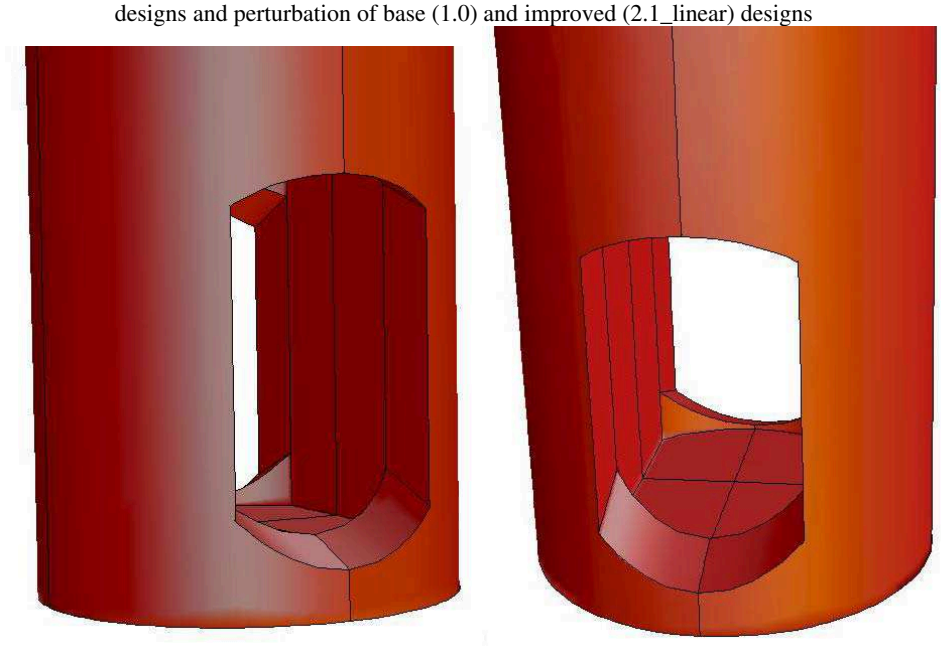

Figure 11. Geometry of improved design 2.1_linear (Port height, p = 80mm; Well angle, α = -20degrees, Well depth, w = 1mm)

7. Conclusions

The paper presented a case study of the design optimization of a continuous caster refractory component, namely a Submerged Entry Nozzle (SEN). The resulting design exhibited a slight improvement in the multi-objective value used, but had superior performance to the base design when its design variables were perturbed. The CFD model results were validated using scale water model tests. The design optimization process was automated using the scripting capability of Fluent and Gambit.

8. References

1. Joo, S, Han, J.W. and Guthrie, R.I.L., Inclusion behavior and heat-transfer phenomena in steelmaking tundish operations, Metallurgical and Materials Transactions B, 1993, 24B: 767.
2. Chakraborty, S. and Sahai, Y., Mathematical modelling of transport phenomena in continuous casting tundishes, Ironmaking & Steelmaking, 1992, 19(6): 479.
3. He, Y. and Sahai, Y., 1987, The effect of tundish wall inclination on the fluid flow and mixing: A modeling study, Metallurgical Transactions B, 18: 81.
4. Huang, X., Thomas, B.G. and Najjar, F.M., 1992, Modeling superheat removal during continuous casting of steel slabs, Metallurgical Transactions B, 23B: 339.
5. Thomas, B.G., O'Malley, R., Shi, T., Meng, Y., Creech, D. and Stone, D., Validation of fluid flow and solidification simulation of a continuous thin-slab caster, Proc. of Conference held August 2000, Aachen, Germany, 769 – 776.
6. Bai, H. and Thomas, B.G., Turbulent flow of liquid steel and argon bubbles in slide-gate tundish nozzles: Part I. Model development and validation. Metallurgical and Materials Transactions B, 2001, 32B: 253.
7. Bai, H. and Thomas, B.G., Turbulent flow of liquid steel and argon bubbles in slide-gate tundish nozzles: Part II. Effect of operation conditions and nozzle design, Metallurgical and Materials Transactions B, 2001, 32B: 269.
8. Mazumdar, D., Yamanoglu, G., Shankarnarayanan, R. and Guthrie, R.I.L., Similarity considerations in the physical modelling of steel making tundish systems, Steel Research, 1995, 66(1): 14.
9. Saha,i Y. and Ahuja, R., Fluid flow and mixing of melt in steelmaking tundishes, Ironmaking & Steelmaking, 1986, 13(5): 241.
10. López-Ramírez, S., Barreto, J. De J., Palafox-Ramos, J., Morales, R.D. and Zacharias, D., Modeling study of the influence of turbulence inhibitors on the molten steel flow, tracer dispersion, and inclusion trajectories in tundishes, Metallurgical and Materials Transactions B, 2001, 32B: 615.
11. Koria, S.C. and Singh, S., Physical modeling of the effects of the flow modifier on the dynamics of molten steel flowing in a tundish, ISIJ International, 1994,, 34(10): 784.
12. Sheng, D.Y. and Jonsson, L., Investigation of transient fluid-flow and heat-transfer in a continuous-casting tundish by numerical-analysis verified with nonisothermal water model experiments, Metallurgical and Materials Transactions B, 1999, 30B(5): 979.
13. De Kock, D.J., Craig, K.J. and Pretorius, C.A., Mathematical Maximisation of the Minimum Residence Time for a Two-Strand Continuous Caster, Ironmaking & Steelmaking, 2003, 30(3): 229-234.
14. Craig, K.J., De Kock, D.J., Makgata, K.W. and De Wet, G.J., Design Optimization of a Single-Strand Continuous Caster Tundish Using RTD Data, ISIJ International, 2001, 41(10): 1194-1200.
15. FLUENT Version 6.0, 6.1, Fluent Inc., Lebanon, NH, USA, www.fluent.com, 2002-4.
16. GAMBIT Version 2.0, 2.1, Fluent Inc., Lebanon, NH, USA, www.fluent.com, 2002-4.
17. Stander, N., Eggleston, T.A., Craig, K.J., Roux, W.J., 2003, LS-OPT v2 User's Manual, Livermore Software Technology Corporation, Livermore, USA.